Intraluminal Cell Transplantation Prevents Growth and Rupture in a Model of Rupture-Prone Saccular Aneurysms

Serge Marbacher, MD, MSc; Juhana Frösén, MD, PhD; Johan Marjamaa, MD, PhD; Andrey Anisimov, PhD; Petri Honkanen, MD†; Michael von Gunten, MD; Usama Abo-Ramadan, PhD; Juha Hernesniemi, MD, PhD; Mika Niemelä, MD, PhD

Background and Purpose—Aneurysm occlusion by intraluminal thrombus formation is the desired effect of all endovascular treatments. Intraluminal thrombus may, however, recanalize and be absorbed, unless it is infiltrated by cells that turn it into fibrous tissue (neointima). Because ruptured aneurysm walls are characterized by loss of smooth muscle cells, we assessed the impact of mural cell loss on wall remodeling of thrombosed aneurysms and investigated whether neointima formation could be enhanced by direct transplantation of cells into the thrombus.

Methods—Sidewall aneurysms were microsurgically created in rats (n=81). Certain aneurysms were decellularized. Thrombosis was induced using direct injection of a fibrin polymer into the aneurysm. CM-Dil–labeled smooth muscle cells were injected into 25 of 46 fibrin embolized aneurysms. Recanalization and aneurysm growth were monitored with magnetic resonance angiography. Endoscopy, optical projection tomography, histology, and immunohistochemistry were used to study the fate of transplanted cells, thrombus organization, and neointima formation.

Results—Decellularized embolized aneurysms demonstrated higher angiographic recurrence compared with decellularized embolized aneurysms with transplanted cells (P=0.037). Local cell replacement at the time of thrombosis resulted in better histological neointima formation than both nondecellularized embolized aneurysms (P<0.001) and decellularized embolized aneurysms (P=0.002). Aneurysm growth and rupture were observed exclusively in decellularized embolized aneurysms.

Conclusions—Lack of smooth muscle cells in the aneurysm wall promotes wall degradation, aneurysm growth and rupture, even if the aneurysm is occluded by luminal thrombus. Transplantation of smooth muscle cells into the luminal thrombus can reduce this degenerative remodeling. **(*Stroke*. 2014;45:3684-3690.)**

Key Words: cell transplantation ■ degeneration ■ inflammation ■ intracranial aneurysm ■ myofibroblasts ■ smooth muscle cells ■ thrombosis

Inducing flow stasis-mediated luminal thrombosis of saccular intracranial aneurysms (IAs) is the goal of all current neuroendovascular treatments. Ideally, the intraluminal thrombus results in immediate exclusion of the aneurysm from circulation, promotes re-endothelialization, and serves as scaffold for recruitment of cells that synthesize extracellular matrix and turn the clot into fibrotic scar tissue (neointima). This cell-mediated remodeling process eventually leads to permanent occlusion of the aneurysm and reconstitution of the luminal surface of the arterial segment harboring the aneurysm.

Thrombolytic cascades are activated at the same time as the coagulation cascade. The luminal thrombus in an aneurysm may therefore eventually be recanalized and reabsorbed if neointima formation and re-endothelialization of the aneurysm ostium do not occur. Growing evidence indicates that the balance between healing and reverse remodeling is mainly determined by the condition of the aneurysm wall.[1–4] Loss of cells from the aneurysm wall is characteristic to ruptured human IAs.[5–7] Previously it has been shown in models of fusiform aortic aneurysms that restoration of the cell content of the aneurysm with local cell transplantation can reduce the progression of the aneurysm.[8,9]

We investigated the hypothesis that loss of mural cells will promote degenerative remodeling of the saccular aneurysm wall in thrombosed aneurysms, and that this degenerative remodeling can be reduced or compensated by direct transplantation of smooth muscle cells (SMCs) into the luminal thrombus.

Received July 19, 2014; final revision received September 20, 2014; accepted September 24, 2014.

From the Department of Neurosurgery, Neurosurgery Research Group, Biomedicum Helsinki, Helsinki University Central Hospital, Helsinki, Finland (S.M., J.F., J.M., P.H., J.H., M.N.); Wihuri Research Institute, Translational Cancer Biology Program, Biomedicum Helsinki (A.A.) and Department of Neurology, Institute of Biomedicine, Experimental MRI Laboratory (U.A.-R.), University of Helsinki, Helsinki, Finland; and Institute of Pathology Laenggasse, Bern, Switzerland (M.v.G.).

†Deceased.

The online-only Data Supplement is available with this article at http://stroke.ahajournals.org/lookup/suppl/doi:10.1161/STROKEAHA.114.006600/-/DC1.

Correspondence to Serge Marbacher, MD, MSc, Neurosurgery Research Group, Biomedicum Helsinki, University of Helsinki, Helsinki, Finland. E-mail serge.marbacher@ksa.ch

Materials and Methods

Animals, Study Design, and Anesthesia

A total of 81 rats were used for this study. Male Wistar rats (Harlan, Horst, The Netherlands) weighing 290 to 400 g served either as experimental pilots (n=10, fibrin polymer induced thrombosis; n=8, optical projection tomography tissue processing and staining protocols) or were randomly allocated to 1 of the 3 groups: thrombus induction in healthy nondecellularized aneurysms (n=17), sick decellularized aneurysms (n=21), and sick decellularized SMC-transplanted aneurysms (n=25). We did not study 1 single group of rats with repeated follow-up contrast-enhanced (CE) MRI, but rather 3 different subgroups representing different time points (groups at days 3, 7, and 21) within each experimental group. After interim analysis, a replication of experiments was performed for time point day 7 (n=4, for all groups). Animals were excluded from final histological analysis when autopsy could not be performed within 12 hours. Study design, drop outs, follow-up modalities, and schedule are given in Figure 1. Surgical characteristics are given in Table I in the online-only Data Supplement.

Aneurysm Model, Graft Decellularization, and Thrombus Induction

Sidewall aneurysms were created under operating microscope by microsurgical end-to-side anastomosis of an arterial saccular graft from the descending thoracic aorta of syngeneic donor rat to the infrarenal abdominal aorta of the recipient animal, as described in detail in the Methods in the online-only Data Supplement.

The untreated donor grafts were immediately reimplanted in thrombus-induced nondecellularized aneurysms rats. The saccular aneurysms to be decellularized before use in thrombus-induced decellularized aneurysms and thrombus-induced decellularized smooth muscle cell–transplanted aneurysms groups were processed as described in detail previously.[10,11] Briefly, donor grafts were harvested and frozen in PBS at −4°C. The next day the grafts were thawed, incubated for 10 hours at 37°C in 0.1% sodium dodecyl sulfate (SDS), and finally refrozen until use. Thrombus induction was performed using fibrin polymer according to the manufacturer's protocol (Tisseel, Baxter). All saccular aneurysms were maximally filled with fibrin clots with or without SMC. To standardize thrombus induction, fibrin clot was carefully aligned with the orifice of the graft leaving no neck remnant. To minimize group differences in hemodynamics, rate of thrombosis and potential recanalization rate, we standardized surgical procedures including aneurysm dimensions and created anastomosis perpendicular to the parent artery (see Methods in the online-only Data Supplement).

Cell Culture, Labeling, and Immunofluorescence

Primary cell cultures were obtained using freshly isolated cells from abdominal aorta segments from the same breeder as the recipient Wistar rats. Although not strictly syngeneic, the histocompatibility is sufficient to avoid graft rejection immune response. Cells were grown, maintained, and underwent 6 to 10 passages before transplantation. Further details of SMC culture are given in the Methods in the online-only Data Supplement. Cells were labeled using a carbocyanine lipid cell membrane tracer (CellTraker CM-Dil, life

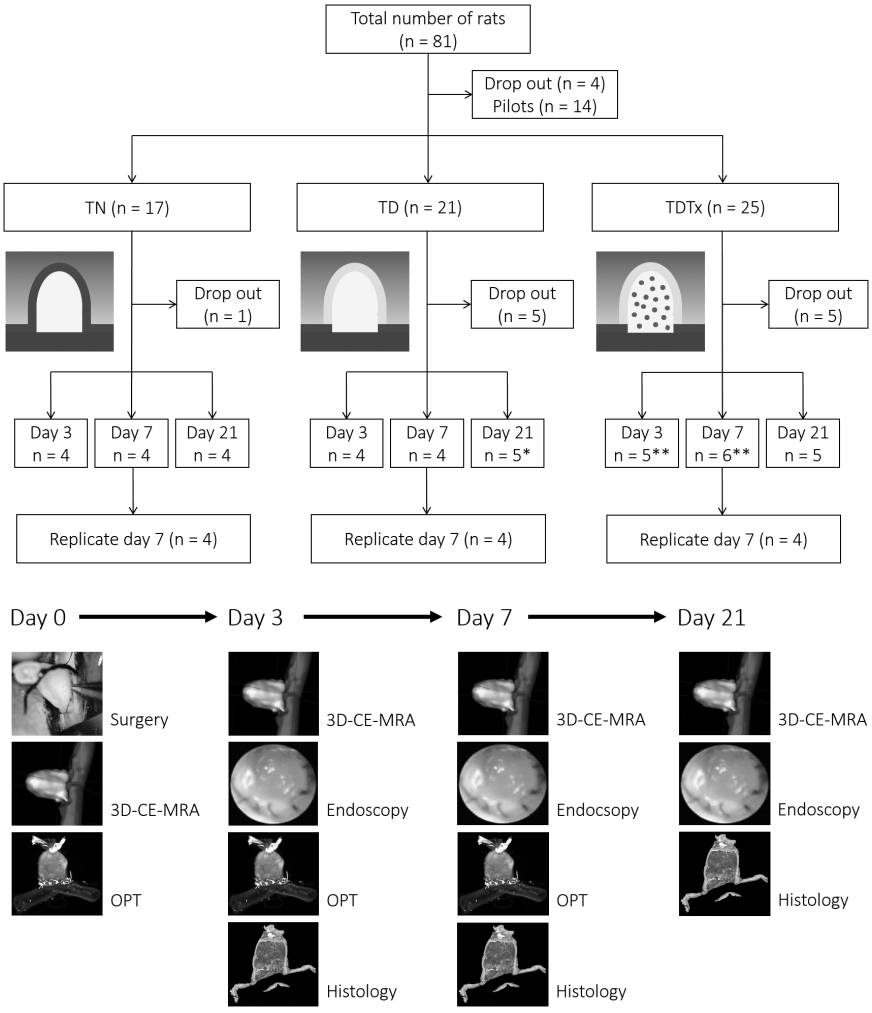

Figure 1. Flowchart of the study design and follow-up modalities. 3D-CE-MRA indicates three-dimensional contrast-enhanced magnetic resonance angiography; TD, thrombus-induced decellularized aneurysms; TDTx, thrombus-induced decellularized smooth muscle cell transplanted aneurysms; and TN, thrombus-induced nondecellularized aneurysms. *One ruptured aneurysm and **2 aneurysms followed up by optical projection tomography (OPT).

Technologies; Invitrogen), homogenously suspended in thrombin solution in a concentration of 1×10^6 cells/mL and mixed with the fibrinogen component to form a clot. The switch from the contractile to the synthetic SMC phenotype (myofibroblast cell phenotype) was confirmed by immunostaining of cytoplasmic smooth muscle actin and vimentin (Figures I–III and Methods in the online-only Data Supplement).

MRI and Angiographic Evaluation

Contrast-enhanced (CE) magnetic resonance angiography (MRA) studies were performed with a 4.7 T scanner (PharmaScan, Bruker BioSpin, Ettlingen, Germany). Existing protocols for high-resolution time-of-flight MRA[12] and CE-MRA[11] were performed. CE-MRA were analyzed and scored for the rate of thrombosis as described previously, with slight modification (Figure IV in the online-only Data Supplement)[11,13]: 0=no recurrence (no filling); 1=partial recurrence (<50% filling); and 2=complete recurrence (>50% filling). Growing aneurysms were further analyzed using 3-dimensional active contour segmentation software itk-SNAP (V2.4, Pennsylvania, PA).[14]

Tissue Preparation and Combined Macroscopic and Endoscopic Scoring

After final follow-up MRA, the animals underwent laparotomy and dissection of the aneurysm (Movie I in the online-only Data Supplement). The tissues were perfusion fixed with 4% paraformaldehyde in PBS and measured in all dimensions. The posterior wall of the aorta was opened and evaluated by macroscopic and endoscopic intraluminal aneurysm surface inspection (Leica Stereomicroscope, Wetzlar, and Karl Storz Endoscopy, Tuttlingen, Germany). Neointima formation was graded as described previously, with slight modification (Figure V in the online-only Data Supplement)[15]: 0=thick neointima, no recanalization, completely sealed; 1=thick neointima, minimal recanalization; 2=thin neointima covering completely; 3=deficient neointima or recurrent aneurysm; and 4=no neointima or complete recanalization. Each case underwent observer-blinded analysis of neointima formation based on ≥1 macroscopic and endoscopic video screen-shot by S.M. and P.H. Scores were dichotomized as complete or near-complete occlusion (scores, 0–1) and incomplete occlusion (scores, ≥2), and compared using the Fisher exact test.

Histology and Histological Analysis

Aneurysms were stained for hematoxylin–eosin, Elastica van Gieson, and Masson–Goldner trichrome. Fluorescent images were examined to determine the fate of transplanted CM-Dil–labeled SMC. All histological slides underwent qualitative analysis by 2 observers (J.F. and S.M.) as described in detail in the Methods in the online-only Data Supplement. Histological scoring was performed blinded for treatment allocation. Slides were visualized under light microscope (Carl Zeiss) and fluorescence microscope (Axiovision, Carl Zeiss). Postprocessing was performed using Adobe Photoshop CS 6 (V13.0, Adobe Systems) and Image J 1.47e (National Institutes of Health, Bethesda, MD) software.[16]

Optical Projection Tomography

Spatial migration of CM-Dil–labeled SMCs was followed up for 1 week after transplantation using optical projection tomography (Bioptonics OPT 3001).[17] Aneurysm and parent artery were stained using in vivo lectin perfusion and visualized in Bioptonics viewer (v2.01, Bioptonics). Three-dimensional animations were created using Imaris 7 (Bitplane Scientific Software; Figure VI and Movie II in the online-only Data Supplement).

Data Analysis and Statistics

Two-tailed Fisher exact test was used for comparison of dichotomized histological, macroscopic and endoscopic grades, and aneurysm growth and recurrence rate between thrombus-induced nondecellularized aneurysms and thrombus-induced decellularized aneurysms, thrombus-induced nondecellularized aneurysms and thrombus-induced decellularized smooth muscle cell–transplanted aneurysms, and thrombus-induced decellularized aneurysms and thrombus-induced decellularized smooth muscle cell–transplanted aneurysms, respectively. Student *t* test was performed to assess differences in surgical characteristics. Data were analyzed and visualized using Graph Pad Prism statistical software V6.04 for Windows (GraphPad Software, San Diego, CA). Values are expressed as mean±SD and 95% confidence interval. A probability value of <0.05 was considered statistically significant.

Results

Luminal thrombus was successfully induced by fibrin polymer injection in all aneurysms with the exception of 1 decellularized aneurysm and 2 cases of decellularized and cell-transplanted aneurysm. In these 3 cases, the aneurysm healed completely (complete fibrin clot reorganization). There was endothelial cell loss in all groups. There was a complete decellularization of all SDS-treated aneurysm grafts without microscopic changes in the extracellular matrix. Case-by-case analysis of macroscopic and endoscopic findings including baseline and follow-up CE-MRA of all animals in all groups including replicates and drop outs are summarized in Figure VII in the online-only Data Supplement.

Recanalization, Growth, and Wall Structure in Embolized Aneurysms With a Healthy Wall

All but 1 aneurysm (1/4) showed partial or complete recurrence after 3 weeks. With the exception of 1 case, all aneurysms showed incomplete neointima formation (Figure 2). In the replication series, half of the aneurysms (2/4) recurred and remained stable. Almost half (5/12) of healthy nondecellularized aneurysm walls showed complete loss (n=3) or only a few remaining viable cells (n=2). Aneurysms with an initially healthy wall that suffered mural cell loss showed significant more wall inflammation and a trend to more neutrophil accumulation in the thrombus when compared with aneurysms without loss of mural cells (P=0.01 and P=0.072; Table II in the online-only Data Supplement). Two of 3 growing aneurysms demonstrated complete mural cell loss.

Recanalization, Growth, and Wall Structure in Embolized Aneurysms With a Sick Wall

First recurrence was seen 7 days after thrombus induction. After 3 weeks, all decellularized aneurysms were partially or completely recanalized. Three aneurysms had grown including 1 aneurysm that grew into a giant partially thrombosed multilobulated aneurysm (Figure VIII in the online-only Data Supplement). One of the growing aneurysms ruptured 10 days after creation. With the exception of 2 cases (2/8), neointima formation was incomplete in all decellularized aneurysms. In the replication series, half of the aneurysm (2/4) demonstrated recurrence and growth. All aneurysms that had experienced growth demonstrated (1) enhanced endoluminal and intrathrombus neutrophil accumulation, (2) inflammatory and hemorrhagic transformation of the wall, and (3) enhanced periadventitial fibrosis (Figure IX in the online-only Data Supplement).

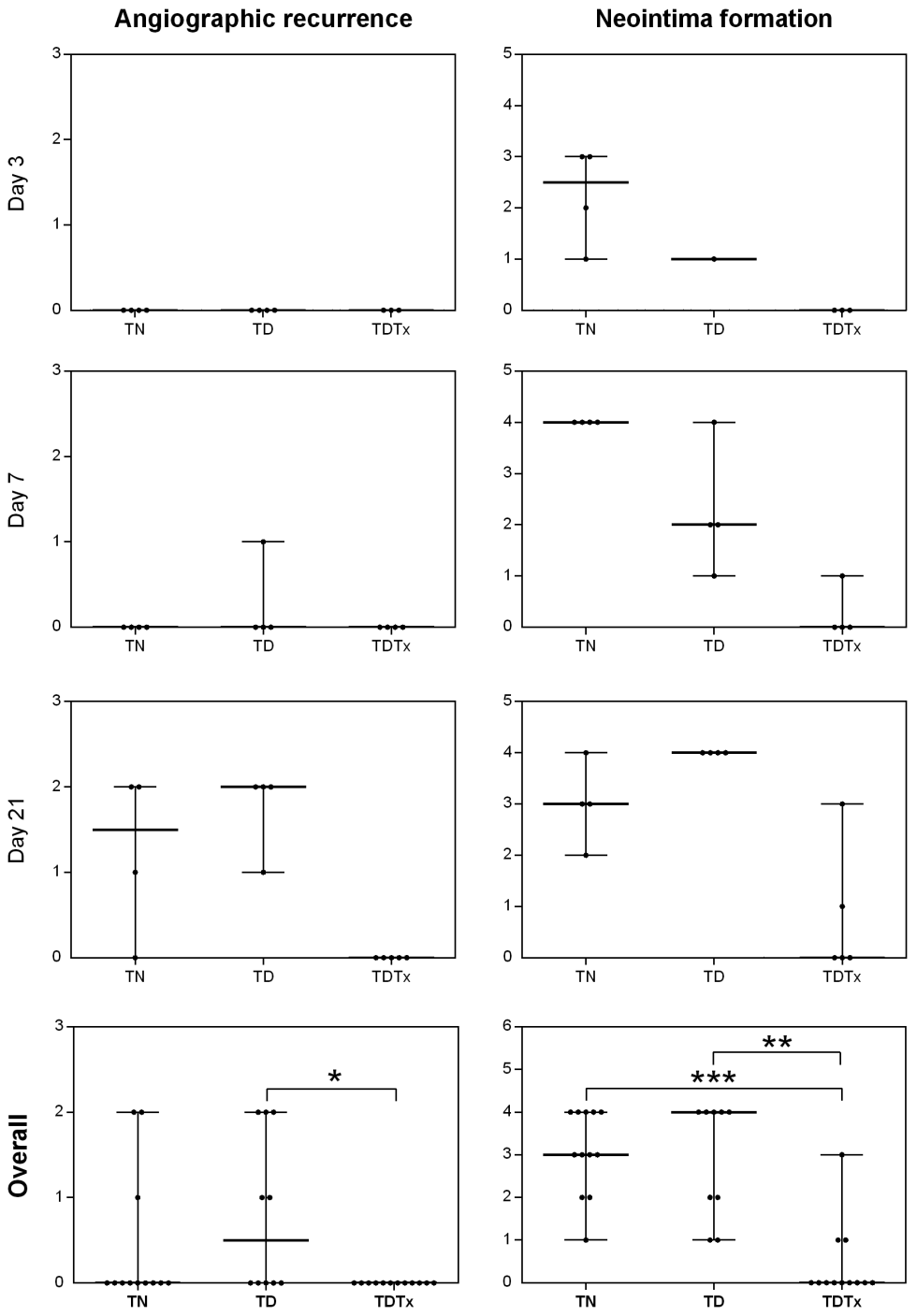

Figure 2. Magnetic resonance angiography recurrence and macroscopic neointima score. TD, thrombus-induced decellularized aneurysms; TDTx, thrombus-induced decellularized smooth muscle cell–transplanted aneurysms; and TN, thrombus-induced nondecellularized aneurysms. *P=0.037; **P=0.002; and ***P<0.001.

Recanalization, Growth, and Wall Structure After Cell Transplantation in Embolized Aneurysms With a Sick Wall

All cell-transplanted aneurysms with a sick wall remained occluded with complete or near-complete neointima formation in all but 1 aneurysm (1/12). The single case of incomplete neointima formation demonstrated increase in aneurysm size at 3-week follow-up. There was no recurrence or growth in the replicate experiments. Intraluminal cell replacement promoted rapid thrombus organization, neointima formation, and aneurysm healing (Figure 3A). After transplantation, cells were equally distributed within the intraluminal thrombus, became confluent within the fibrin clot, and demonstrated no trend of migration toward the aneurysm wall or the aneurysm ostium (Figure 3B). Spindle-shaped CM-DiI–labeled cells embedded in collagen bundles were found to organize the fibrin clot and neointima along the neck (Figure 4).

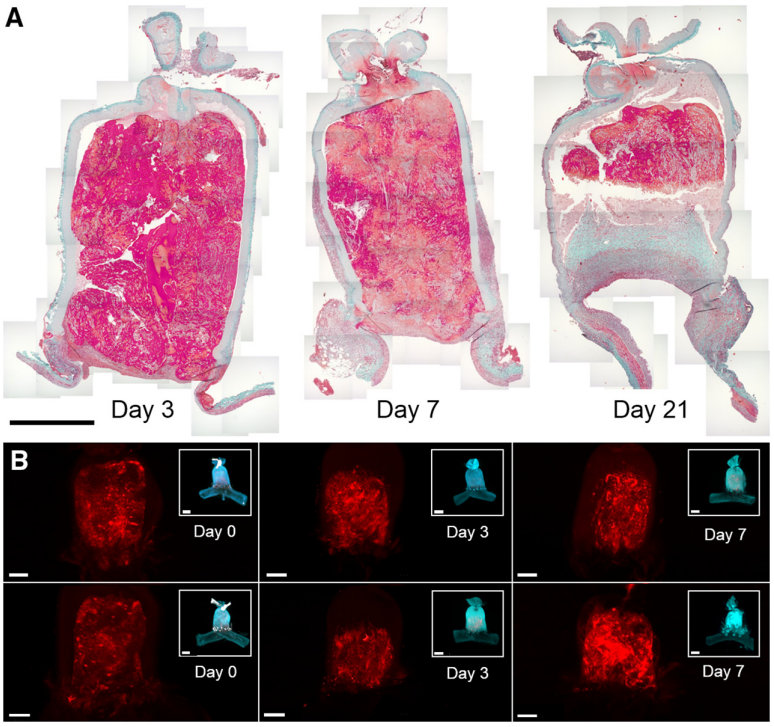

Figure 3. Time course of aneurysm healing. **A**, Three days after cell graft placement, organization of the fibrin clot and neointima formation starts. Already after 1 week, organization progresses and thick neointima is formed at the aneurysm orifice. In week 3, the ostium is completely occluded by thick neointima and large amounts of collagen deposits. Merged Masson trichrome–stained photomicrographs (magnification ×10); scale bar, 1 mm. **B**, Optical projection tomography reveals inner structure of the aneurysm and spatial distribution of transplanted cells over time. Labeled cells appear in bright red (Texas Red filter, CM-Dil staining, main panel, scale bars, 500 μm). The entire aneurysm and part of its parent artery are displayed in translucent greenish-blue (green fluorescent protein and green fluorescent protein+filter, autofluorescence and fluorescein isothiocyanate lectin staining, inset top right, scale bars, 1000 μm).

Comparison of Thrombus-Induced and Cell-Transplanted Aneurysms With Thrombus-Induced Aneurysms Without Cell Transplantation

Overall recurrence rate of thrombus-induced sick decellularized aneurysms was significantly higher when compared with thrombus-induced sick decellularized aneurysms with concomitant cell replacement (P=0.037). Decellularized aneurysm treated with local cell replacement at the time of thrombosis demonstrated significantly superior histological neointima formation than thrombus-induced healthy nondecellularized aneurysms (P<0.001) and thrombosed sick decellularized aneurysms (P=0.002).

There was significantly more neutrophil accumulation in the thrombus in decellularized aneurysms (P=0.03) and a trend (P=0.15) toward increased neutrophils in the thrombus of nondecellularized aneurysms as compared with decellularized aneurysms with local cell transplantation (Figure X in the online-only Data Supplement). Healed aneurysm had significantly less neutrophils in the thrombus as compared with aneurysms with missing neointima formation (P=0.017; Table III in the online-only Data Supplement).

Discussion

Our results demonstrate that loss of SMC in the aneurysm wall impairs thrombus organization and neointima formation in thrombosed aneurysms and promotes recurrence, growth, and eventual rupture of embolized aneurysms. Furthermore, our results suggest that thrombus induction in healthy aneurysms can provoke mural cell loss and increase intramural and intrathrombus inflammation. Local cell transplantation to the thrombus enhances thrombus organization, compensates for the loss of mural cells, attenuates inflammatory reactions, promotes aneurysm healing, and reduces recurrence, growth, and rupture rate of thrombosed aneurysms.

The sidewall aneurysm model only partially reflects the actual pathogenesis of human IA. The model allows to study basic biological concepts although one needs to be aware of differences in hemodynamic characteristics and vascular biology between the aorta and cerebral arteries. None of the

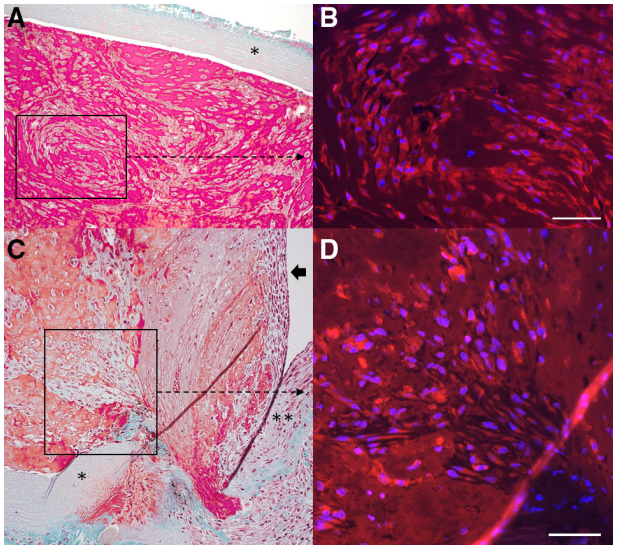

Figure 4. Fibrin clot organization and neointima formation. **A** and **B**, Three days after transplantation: (**A**) Masson–Goldner trichrome (MT) staining demonstrates many cells trapped in the fibrin clot and beginning of spatial organization of the cells without collagen deposits (magnification ×10). *Decellularized aneurysm wall. **B**, The presence of DiI-labeled spindle-shaped cells within the fibrin clot (magnification ×10); scale bar, 50 μm. **C** and **D**, Seven days after transplantation: (**C**) MT staining displays connective tissue formation and formation of a thick layer of hypercellular tissue across the aneurysm's neck (black arrow; magnification ×10). **Healthy parent artery wall. **D**, Detection of labeled cells in areas of collagen formation (magnification ×20); scale bar, 50 μm.

available aneurysm models that can be embolized ideally represent a human saccular cerebral artery aneurysm or reproduce the exact pathobiology behind aneurysm formation or rupture.

The models developed by Hashimoto et al[18] are the most physiological IA models to date in terms of representing human morphology, histology, and IA hemodynamics. Because we assessed the impact of mural cell loss on wall remodeling of thrombosed aneurysms, we performed the experiments in the presented saccular sidewall model, which allowed us to induce thrombosis and perform cell transplantation in arterial grafts with different wall conditions (cell-rich healthy and decellularized sick walls).

Aneurysm Wall Condition Predicts Natural Course and Fate of Intraluminal Thrombosis

MRA, macroscopic and microscopic evaluation, and histology of aneurysms with loss of mural cells revealed their inability to organize induced thrombosis. Initially healthy aneurysms that suffered mural cell loss because of rapid intraluminal thrombus induction showed an evolution similar to sick decellularized aneurysms in terms of recurrence, growth, and increase in wall inflammation and intrathrombus neutrophil accumulation. Taken together, the findings corroborate previous experimental research suggesting that neointimal SMCs originate from the wall of the aneurysm[1] and that aneurysms missing mural cells are subject to increased inflammatory reaction, severe wall degeneration, aneurysm growth, and eventual rupture.[11]

If the experimental findings holds true for the human IA wall it would mean that decreased number of SMCs would be a potential surrogate marker for not only prediction of rupture risk but also estimation of healing response after embolization. Macrophage imaging within human cerebral aneurysm walls using ferumoxytol-enhanced MRI demonstrated that knowledge of the histological correlation of aneurysm risk can be valuable for clinical decision making. In human histopathologic series loss of mural SMCs was found to be even more characteristic for rupture-prone aneurysm wall than inflammation.[6,7]

Local Cell Therapy Heals Aneurysms With Degenerated/Decellularized Walls

The findings demonstrate that transplanted viable SMCs compensate the loss of mural cells and improve early thrombus reorganization and neointima formation. Neointima formation prevents recurrence and additional thrombus formation. Consequently, intraluminal amount of new red blood cells, platelets, and macromolecular plasma components such as lipids, complement, and immunoglobulins are reduced, which in turn attenuates wall inflammation. This could explain the finding that healed aneurysm had significantly fewer neutrophils in the thrombus as compared with aneurysms with missing neointima formation.

The compensation of mural SMC loss by local cell therapy may have great therapeutic potential. It has been demonstrated that bone marrow mesenchymal stem cell and SMC transplantation can stabilize growing abdominal aortic aneurysms in rats[8,9] and promote healing of saccular venous pouch aneurysms in dogs.[19] In a rabbit model of elastase-induced saccular aneurysms, endovascular seeding of bone marrow mesenchymal stem cells promoted thrombus organization and caused the aneurysm to shrink in size.[20] For a more detailed discussion of potential cell-mediated methods to promote aneurysm wall healing and repair please see our prior review.[21]

Limitations

In previous experiments, spontaneous stepwise thrombosis did not result in increased inflammation, mural cell loss in healthy aneurysms, and did not promote aneurysm growth or rupture.[11] A potential explanation for these (contradictory) findings might be that acute thrombosis induces inflammation on such a large scale that it over-runs the aneurysm wall defense mechanisms or that fibrin biopolymer leads to a thicker clot than normal coagulation. Acute thrombus induction has been linked to mural destabilization not only in experimental aneurysms[22,23] but also in the clinical setting after application of flow diverters to treat intracranial aneurysms.[24,25] These studies consistently found histopathologic characteristics comparable with those found in our study, with large amounts of inflamed cells and mural cells loss in destabilized aneurysm wall segments after rapid thrombosis.[22,23,25]

However, the cell loss observed in healthy aneurysms could also be attributed to ischemic or inflammatory reactions induced by the fibrin polymer thrombus. It might also be possible that luminal fibrin polymer lead to a thicker clot than normal coagulation and impaired diffusion of nutrients to the healthy media and promoted inflammation as a secondary reaction. In future experiments it would be of much interest to study the course of clinically more relevant coil-induced thrombosis in decellularized and healthy (cell-rich) aneurysms.

Hemodynamic characteristics, rate of spontaneous thrombosis and recanalization, and healing/remodeling processes after intraluminal thrombosis are significantly influenced by the experimental aneurysm angioarchitecture.[13,26,27] Despite the efforts made to standardize aneurysm dimensions, we cannot exclude completely the possibility of group differences in hemodynamics and hence rate of thrombosis and recanalization.

Conclusions

The present study provides additional evidence that the condition of the aneurysm wall is of utmost importance for the net effect that a thrombus has on aneurysm healing. Methods that can be used in the clinical setting to evaluate the number and function of mural SMCs may significantly help in the diagnostics of rupture-prone IA and in prediction of accuracy of healing capacity after embolization. Novel therapies that increase the number of functioning SMC could compensate for mural cell loss and reduce the recurrence, growth, and rupture rate of IA and may also improve the healing capacity after intraluminal thrombus induction.

Acknowledgments

We thank N. Lim and O. Mattila for their excellent technical assistance. We thank J. Kenkkila for support in optical projection tomography (OPT) imaging acquisition, image processing, and in 3-dimensional contrast-enhanced magnetic resonance angiography volumetry. We thank G.V.D. Amico Lago for sharing her expertise in OPT tissue processing. We thank T. Holopainen for sharing her expertise for in vivo fluorescein isothiocyanate lectin staining. We are grateful to A. Reijula and M. Berthold for tissue processing and staining. The Biomedicum Molecular Imaging Unit is acknowledged for microscopy services. We are grateful for the support of the Kari Alitalo laboratory for cell culture staining. Dr Marbacher contributed to the study concept, performed the experiments, analyzed the data, prepared the figures, obtained personal funding, and wrote the article. Dr Frösén developed the study concept, helped to perform initial surgical experiments, provided expertise in cell culture and pathology, analyzed the histopathology, and helped to write the article. Dr Marjamaa performed surgical experiments and provided expertise in MRI. Dr Anisimov provided expertise in cell culture and cellular labeling. Dr Honkanen analyzed macroscopic and endoscopic video screenshots. Dr von Gunten provided expertise in pathology, tissue processing, and staining. Dr Abo-Ramadan performed MR scans and provided expertise in and designed MRI sequences. Drs Hernesniemi and Niemelä directed the studies, provided funding, and helped to write the article.

Sources of Funding

This work was supported by the research funds of the Helsinki University Central Hospital, Helsinki, Finland, and by grants from The Sigrid Juselius Foundation (Helsinki, Finland). Dr Marbacher was supported by a grant from the Swiss National Science Foundation (PBSKP3-123454).

Disclosures

We are solely responsible for the design and conduct of the presented study and report no conflict of interest concerning the materials and methods used in this study or the findings specified in the article. They confirm the adherence of ethical standards. Dr Frösén has received research grants or research support from Cook Medical and speaker honorariums from the European Society for Minimally Invasive Neurological Therapy. The other authors report no conflicts.

References

1. Frösen J, Marjamaa J, Myllärniemi M, Abo-Ramadan U, Tulamo R, Niemelä M, et al. Contribution of mural and bone marrow-derived neointimal cells to thrombus organization and wall remodeling in a microsurgical murine saccular aneurysm model. *Neurosurgery*. 2006;58:936–944, discussion 936.
2. Krings T, Mandell DM, Kiehl TR, Geibprasert S, Tymianski M, Alvarez H, et al. Intracranial aneurysms: from vessel wall pathology to therapeutic approach. *Nat Rev Neurol*. 2011;7:547–559.
3. Frösen J, Tulamo R, Paetau A, Laaksamo E, Korja M, Laakso A, et al. Saccular intracranial aneurysm: pathology and mechanisms. *Acta Neuropathol*. 2012;123:773–786.
4. Chalouhi N, Ali MS, Jabbour PM, Tjoumakaris SI, Gonzalez LF, Rosenwasser RH, et al. Biology of intracranial aneurysms: role of inflammation. *J Cereb Blood Flow Metab*. 2012;32:1659–1676.
5. Frösen J, Piippo A, Paetau A, Kangasniemi M, Niemelä M, Hernesniemi J, et al. Remodeling of saccular cerebral artery aneurysm wall is associated with rupture: histological analysis of 24 unruptured and 42 ruptured cases. *Stroke*. 2004;35:2287–2293.
6. Kataoka K, Taneda M, Asai T, Kinoshita A, Ito M, Kuroda R. Structural fragility and inflammatory response of ruptured cerebral aneurysms. A comparative study between ruptured and unruptured cerebral aneurysms. *Stroke*. 1999;30:1396–1401.
7. Tulamo R, Frösen J, Junnikkala S, Paetau A, Pitkäniemi J, Kangasniemi M, et al. Complement activation associates with saccular cerebral artery aneurysm wall degeneration and rupture. *Neurosurgery*. 2006;59:1069–1076, discussion 1076.
8. Allaire E, Muscatelli-Groux B, Guinault AM, Pages C, Goussard A, Mandet C, et al. Vascular smooth muscle cell endovascular therapy stabilizes already developed aneurysms in a model of aortic injury elicited by inflammation and proteolysis. *Ann Surg*. 2004;239:417–427.
9. Schneider F, Saucy F, de Blic R, Dai J, Mohand F, Rouard H, et al. Bone marrow mesenchymal stem cells stabilize already-formed aortic aneurysms more efficiently than vascular smooth muscle cells in a rat model. *Eur J Vasc Endovasc Surg*. 2013;45:666–672.
10. Allaire E, Guettier C, Bruneval P, Plissonnier D, Michel JB. Cell-free arterial grafts: morphologic characteristics of aortic isografts, allografts, and xenografts in rats. *J Vasc Surg*. 1994;19:446–456.
11. Marbacher S, Marjamaa J, Bradacova K, von Gunten M, Honkanen P, Abo-Ramadan U, et al. Loss of mural cells leads to wall degeneration, aneurysm growth, and eventual rupture in a rat aneurysm model. *Stroke*. 2014;45:248–254.
12. Marjamaa J, Antell H, Abo-Ramadan U, Hernesniemi JA, Niemelä MR, Kangasniemi M. High-resolution TOF MR angiography at 4.7 Tesla for volumetric and morphologic evaluation of coiled aneurysm neck remnants in a rat model. *Acta Radiol*. 2011;52:340–348.
13. Yoshino Y, Niimi Y, Song JK, Khoyama S, Shin YS, Berenstein A. Preventing spontaneous thrombosis of experimental sidewall aneurysms: the oblique cut. *AJNR Am J Neuroradiol*. 2005;26:1363–1365.
14. Yushkevich PA, Piven J, Hazlett HC, Smith RG, Ho S, Gee JC, et al. User-guided 3D active contour segmentation of anatomical structures: significantly improved efficiency and reliability. *Neuroimage*. 2006;31:1116–1128.
15. Raymond J, Salazkin I, Georganos S, Guilbert F, Desfaits AC, Gevry G, et al. Endovascular treatment of experimental wide neck aneurysms: comparison of results using coils or cyanoacrylate with the assistance of an aneurysm neck bridge device. *AJNR Am J Neuroradiol*. 2002;23:1710–1716.
16. Schneider CA, Rasband WS, Eliceiri KW. NIH Image to ImageJ: 25 years of image analysis. *Nat Methods*. 2012;9:671–675.
17. Sharpe J, Ahlgren U, Perry P, Hill B, Ross A, Hecksher-Sørensen J, et al. Optical projection tomography as a tool for 3D microscopy and gene expression studies. *Science*. 2002;296:541–545.
18. Hashimoto N, Handa H, Hazama F. Experimentally induced cerebral aneurysms in rats. *Surg Neurol*. 1978;10:3–8.
19. Raymond J, Desfaits AC, Roy D. Fibrinogen and vascular smooth muscle cell grafts promote healing of experimental aneurysms treated by embolization. *Stroke*. 1999;30:1657–1664.
20. Rouchaud A, Journé C, Louedec L, Ollivier V, Derkaoui M, Michel JB, et al. Autologous mesenchymal stem cell endografting in experimental cerebrovascular aneurysms. *Neuroradiology*. 2013;55:741–749.
21. Frösen J. Smooth muscle cells and the formation, degeneration, and rupture of saccular intracranial aneurysm wall–a review of current pathophysiological knowledge. *Transl Stroke Res*. 2014;5:347–356.
22. Becker TA, Preul MC, Bichard WD, Kipke DR, McDougall CG. Preliminary investigation of calcium alginate gel as a biocompatible material for endovascular aneurysm embolization in vivo. *Neurosurgery*. 2007;60:1119–1127, discussion 1127.
23. Raymond J, Darsaut TE, Kotowski M, Makoyeva A, Gevry G, Berthelet F, et al. Thrombosis heralding aneurysmal rupture: an exploration of potential mechanisms in a novel giant swine aneurysm model. *AJNR Am J Neuroradiol*. 2013;34:346–353.
24. Hampton T, Walsh D, Tolias C, Fiorella D. Mural destabilization after aneurysm treatment with a flow-diverting device: a report of two cases. *J Neurointerv Surg*. 2011;3:167–171.
25. Kulcsár Z, Houdart E, Bonafé A, Parker G, Millar J, Goddard AJ, et al. Intra-aneurysmal thrombosis as a possible cause of delayed aneurysm rupture after flow-diversion treatment. *AJNR Am J Neuroradiol*. 2011;32:20–25.
26. Black SP, German WJ. Observations on the relationship between the volume and the size of the orifice of experimental aneurysms. *J Neurosurg*. 1960;17:984–990.
27. Yoshino Y, Niimi Y, Song JK, Silane M, Berenstein A. Endovascular treatment of intracranial aneurysms: comparative evaluation in a terminal bifurcation aneurysm model in dogs. *J Neurosurg*. 2004;101:996–1003.

Stroke
Journal of the American Heart Association

Intraluminal Cell Transplantation Prevents Growth and Rupture in a Model of Rupture-Prone Saccular Aneurysms

Serge Marbacher, Juhana Frösén, Johan Marjamaa, Andrey Anisimov, Petri Honkanen, Michael von Gunten, Usama Abo-Ramadan, Juha Hernesniemi and Mika Niemelä

Stroke. 2014;45:3684-3690; originally published online November 4, 2014;
doi: 10.1161/STROKEAHA.114.006600
Stroke is published by the American Heart Association, 7272 Greenville Avenue, Dallas, TX 75231

Print ISSN: 0039-2499. Online ISSN: 1524-4628

SUPPLEMENTAL MATERIAL

Methods

Animal preparation and experimental protocol

Animals were housed in the animal room at 22-24°C with a 12-hour light/dark cycle and free access to pellet diet and regular tap water. They received humane care in conformity with institutional guidelines. The experiments were reviewed and approved by the Committee for Animal Welfare at the University of Helsinki, Finland. The rats were anesthetized by a subcutaneous injection of medetomidine hydrochloride (0.5 mg/kg, Domitor; Orion, Espoo, Finland) and intraperitoneal injection of ketamine hydrochloride (50 mg/kg, Ketalar; Parke-Davis, Detroit, MI, USA). Subcutaneous injection of buprenorphine (0.3 mg/kg, Temgesic; Schering-Plough Oy, Espoo, Finland) was used for analgesia.

Sidewall aneurysms were created according to standard operating procedures[1]. The orifice of the arteriotomy of the recipient was tailored to the donor graft to achieve tight aneurysm neck anastomosis. The left inguinal region was dissected, the femoral vein isolated and cannulated (Becton Dickinson and Company, Sparks, MD, USA) for contrast agent (Gd-DOTA) injection and fluid resuscitation (Glucose 5%). A digital video camera (Sony Exwave HAD SSC-DC58AP, Tokyo, Japan) attached to the stereomicroscope (Leica M651, Wetzlar, Germany) was used to document preoperative aneurysm dimensions (width and length), microsurgical anastomosis procedures (total operating time, aortic clamping time, time for anastomosis creation, time to hemostasis, number of extra sutures, graft ischemia time and complications), patency of distal abdominal aorta and aneurysm harvest procedure including follow-up aneurysm dimensions and endoscopic inspection at magnifications between 6x and 40x.

Surgical characteristics, morbidity and mortality

Four animals died during piloting- two rats deceased prior to surgery (anesthesia-related complication) and two during attempts at transvascular embolization. Further dropouts were as follows: TN – one animal died due to air embolism during femoral vein catheter placement on day 0. TD – one animal prior to surgery (anesthesia-related), two animals deceased due to proximal and distal dissection of the aorta on day 9 (the aneurysm angioarchitecture remained unchanged compared to baseline); in one animal, cause of death on day 8 remains unclear (delayed autopsy); one animal perished due to rupture of a growing aneurysm on day 9 (detailed description below). TDTx – one animal died due to thrombosis of the parent artery on day 0; another animal was euthanized after occurrence of bilateral femoral artery thrombosis on day one after surgery; in two animals, cause of death remains unclear (delayed autopsy) on day 10 and 12, respectively; one animal died due to abdominal cavity infection (overlooked gauze pads). Despite randomization there were significant differences in body weight and total operation time between the non-decellularized graft group (TN) and decellularized aneurysm groups (TD and TDTx). The prolonged operation time in animals receiving non-decellularized aneurysms is explained by the delay caused during graft harvesting in simultaneously operated donor rats, while the decellularized grafts were ready for use at the time of surgery. All other assessed surgical characteristics did not differ between the experimental groups.

Cell culture

Primary cell culture cells were obtained by the explant and enzymatic digestion method. A one to two centimeter abdominal aortic segment was excised and cleaned of fat tissue and adventitia with sterile forceps and micro scissors, washed with PBS, transferred to warmed Dulbeco's Modified Eagle's Medium (DMEM, Invitrogen), rinsed and chopped into approximately 1 mm^3 squares. The tissue pieces underwent trypsin digestion for 20 minutes at

37°C followed by incubation in fetal bovine serum (FBS, Gibco®/Invitrogen) for 15 min. After centrifugation, the supernatant was discarded and the tissue evenly distributed in 6-well cell culture cluster (Costar®, Corning, NY, USA) containing DMEM, supplemented with 10% FBS and Penicillin (500 U/mL)-Streptomycin (5mg/ml)-L-Glutamine (5mM) solution (Invitrogen, Life Technologies, CA, USA). The primary cell cultures were passaged initially at a ratio of 1:2 when the cells became confluent. Cells were maintained in 25 and 75 cm^2 tissue culture flasks (Corning, NY, USA) and underwent 6-10 passages before transplantation. Cultures were incubated at 37°C in humified air enriched with 5% CO^2 and fed by exchanging the media two to three times a week.

Cellular labeling

The number of live cells obtained after trypsination were counted prior to labeling. In a typical experiment, the percentage of dead cells did not exceed 1 - 2%. The cells were labeled by incubation in 1ml of 10µM 1,1-dioctadecyl-3,3,3,3-tetramethylindocarbocyanine perchlorate solution (C-7001, Invitrogen/Molecular Probes, Sigma-Aldrich) for 5 minutes at 37°C and for another 15 minutes at 4°C. After labeling, the cells were washed in PBS, centrifuged and homogenously resuspended in the thrombin solution at a concentration of 1 x 106 cells/ml, followed by mixing with the fibrinogen component to form a clot. To determine the intensity of the fluorescence labeling ~50`000 cells of each sample were Cellspin mounted onto slides and analyzed using an Axiovision fluorescence microscope (Carl Zeiss). The nuclei were counterstained with DAPI (component of VECTASHIELD® Mounting Medium, Vector Laboratories) (Supplemental Figure I).

Immunofluorescence in cell culture

Quantification of differentiation of smooth muscle cells into myofibroblasts was assessed by cell culture staining for α-smooth muscle actin and vimentin and viewed with fluorescence microscopy (Axiovision, Carl Zeiss) under 20x magnification (Supplemental Figure II). For immunocytochemical staining, the cells were cultured on coverslips until confluency, fixed with 4% PFA and permeabilized with 0.1% Triton X-100. Fixed cells were stained with the antibodies against human smooth muscle actin (Dako 1:200) and vimentin (Sigma-Aldrich, 1:40). Secondary antibodies were Cy3-conjugated donkey anti-mouse IgG and FITC-conjugated donkey anti-rabbit IgG (Jackson Immuno Research Laboratories). The nuclei were counterstained with DAPI. Cells were imaged using fluorescence confocal microscopy (TCS CARS SP8, Leica Microsystems) in multichannel scanning under 10x and 40x magnification. Negative control staining was performed with species-matching unspecific antibody (Supplemental Figure III).

Magnetic resonance imaging and angiographic evaluation

Magnetic resonance angiography (MRA) studies were performed with a 4.7 T scanner (PharmaScan, Bruker BioSpin, Ettlingen, Germany) using a 90-mm shielded gradient capable of producing maximum gradient Germany amplitude of 300 mT/m with 80-msec rise time. A linear birdcage radiofrequency coil with inner diameter of 60 mm was used. Existing protocols for high resolution TOF-MRA [2] were combined with contrast enhanced angiography (CE-MRA) [3]. All animals underwent high-resolution imaging (postoperative at day 0 and at final follow-up as defined by the respective group) to evaluate flow characteristics, parent vessel integrity, perianeurysmal environment, changes in aneurysm volume, extent of spontaneous thrombosis and recanalization.

After shimming and scout images, the three dimensional fast low-angle shot sequence (3D-FLASH) was acquired (TR/TE=15/2.5 ms, flip angle=20°, field-of-view = 40 × 40 x 40 mm3, matrix size = 256 × 256 x 16 zero filling to 256 × 256 x 256 and acquisition time = 3 min 45 s). Afterwards, the 3D FLASH (TR/TE=15/2.5 ms, flip angle=20°, field-of-view = 40 × 40 x

20 mm3, matrix size = 256 × 128 x 16 zero filling to 256 × 128 x 256 and acquisition time = 1 min 32 s) with short imaging time was performed. At that time, the animals received a bolus injection of Gd-DOTA (1 ml/kg body weight, intravenously, injection time < 3 s) and the 3D FLASH with short imaging time (CE-MRA) repeated twice without delay between the scans (late CE-MRA). In total, MR imaging took approximately 30 minutes.

Aneurysm recurrence was categorized on contrast filling in the aneurysms axial dimension as follows: 0 = no recurrence (no filling); 1 = partial recurrence (< 50%); 2 = complete recurrence (> 50%) (Supplemental Figure IV). Scores were dichotomized as no recurrence (score 0) or recurrence (scores, 1-2) and compared using the Fisher exact test.

High-quality imaging of the perianeurysmal environment, aneurysm and parent artery were obtained in all cases. In three of 116 scans, contrast agent was missing due to technical problems. Parent arteries remained without adverse findings (no dilatation or constriction). Bowel adhesion and perianeurysmal contrast enhancement after early and late CE-MRA occurred irregularly in all three groups. In one case (TD replicate), strong periadventitial and paraspinal muscular inflammation occurred.

Histopathology and histological analysis
After overnight incubation in 4% formalin, the samples were transferred to phosphate buffered saline, dehydrated through a graded ethanol series and embedded in paraffin. Aneurysms embedded in paraffin blocks were cut in the middle along its longitudinal axis and cut into consecutive 4 μm sections for Hematoxylin-Eosin, Elastica van Gieson's, and Masson-Goldner's trichrome staining. Fluorescent images were examined to determine the fate of transplanted CM-Dil labeled myofibroblasts: Ingrowth in luminal thrombosis and organization of thrombosis and fibrin glue, neointima formation, infiltration of the adventitia, ingrowth in periadventitional environment, migration to the parent artery and CM-Dil uptake by macrophage cells.

The following histopathological characteristics were assessed on conventional HE, EVG and MT stained sections, and scored as follows: Periadventitial inflammation (0 = none, 1 = mild, 2 = moderate, 3 = severe), periadventitial fibrosis (0 = none, 1 = mild, 2 = moderate, 3 = severe), aneurysm wall inflammation (0 = none, 1 = few (1-3) spots, 2 = many (>4) spots, 3 = ubiquitous), aneurysm wall hematoma (0 = none, 1 = few (1-3) spots, 2 = many (>4) spots, 3 = ubiquitous), aneurysm wall cellularity (0 = none, 1 = few (1-3) spots, 2 = many (>4) spots, 3 = ubiquitous), aneurysm wall dissection (0 = none, 1 = few (1-3) spots, 2 = many (>4) spots, 3 = ubiquitous), endothelial cellularity (0 = none, 1 = few (1-3) spots, 2 = many (>4) spots, 3 = ubiquitous), luminal thrombus (0 = absent, 1 = present), neutrophils in the thrombus (0 = none, 1 = mild, 2 = moderate, 3 = severe), and neointima formation (0 = none, 1 = organizing thrombus, 2 = organizing thrombus and neointima formation, 3 = mature neointima). Scores were dichotomized as (1) none/mild and moderate/severe, (2) no/few cells and focal hypo-cellularity/normal cell count and (3) no neointima/organizing thrombus and organizing neointima/mature neointima.

Optical projection tomography
In-vivo Lectin perfusion and tissue processing. Cell transplantation experiments were carried out as described above. On day 0, 3, and 7, 200ul Fluorescein isothiocyanate (FITC)-conjugated Lycopersicon esculentum (tomato) lectin (Sigma-Aldrich, St. Louis, MO) diluted in 200ul PBS was injected into the femoral vein and allowed to circulate for 5 min. Rats were kept on a comfortable warm heat block after injection and before receiving a lethal dose of xylazine-ketamine. Intracardiac perfusion-fixation was carried out at room temperature with PBS followed by 4% PFA in PBS. Specimens were removed from the abdominal cavity and

immersed in 4% paraformaldehyde at 4°C overnight, then embedded in 1% low-melt agarose. Samples were mounted on rotary stages, dehydrated in 75% methanol and subsequently cleared using a 1:2 mixture of benzyl alcohol and benzyl benzoate over a 72 hour period.

Data acquisition and visualization. Optical projection tomography (Bioptonics OPT 3001) was applied to scan the aneurysms stepwise at 0.9 degrees resulting in 400 images of projection data over one complete revolution. Images were taken with the following filters: WL (withe light; visualization of suture material – assigned color white), GFP1 (425/40 nm exciter, 475 nm emitter; autofluorescence; visualization of fibrin biopolymer induced thrombus – assigned color yellow), GFP+, (470/40 nm exciter, 515 nm emitter; FITC-lectin; visualization of vessel wall – assigned color blue), and TXR (560/40 nm exciter, 610 nm emitter; CM-Dil; visualization of transplanted cells – assigned color red). Post alignment was carried out on at least three levels through the specimen, and image stacks were reconstructed using NRecon software (v1.6.3.3, Skyscan) and three dimensional volumetric representations visualized in Bioptonics viewer (v2.01, Bioptonics). Automated object detection (transplanted cells and vessel wall) and isosurface rendering in maximal intensity projections was performed to create 3D animations using image processing software Imaris 7 (Bitplane Scientific Software, Andor Technology) (Supplemental Figure VI and Supplemental Movie II).

Supplemental Figure I - Cellular labeling.

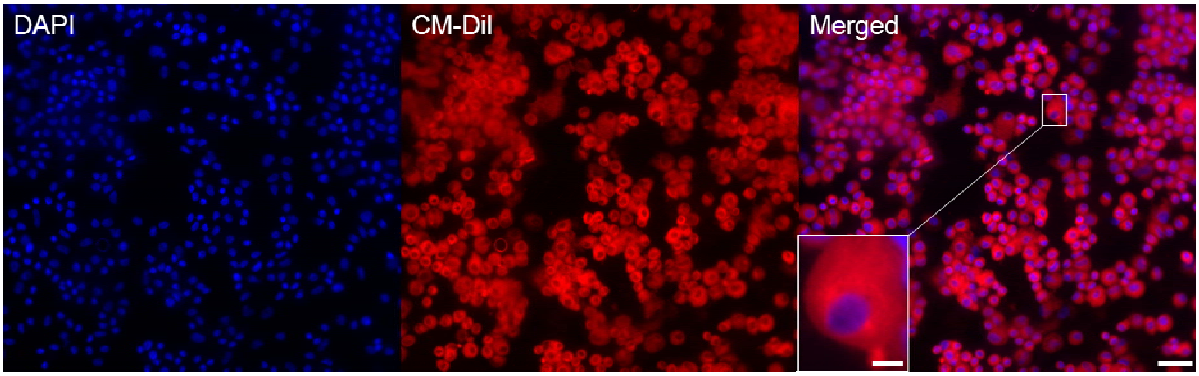

Representative fluorescent photomicrograph of Cellspin mounted samples of CM-Dil stained cells. Nuclei were counterstained with DAPI. Almost all nucleated cells are labeled with CM-Dil. 20x magnification. Scale bar = 50 µm. Inlet scale bar = 10 µm.

Supplemental Figure II - Cell culture staining.

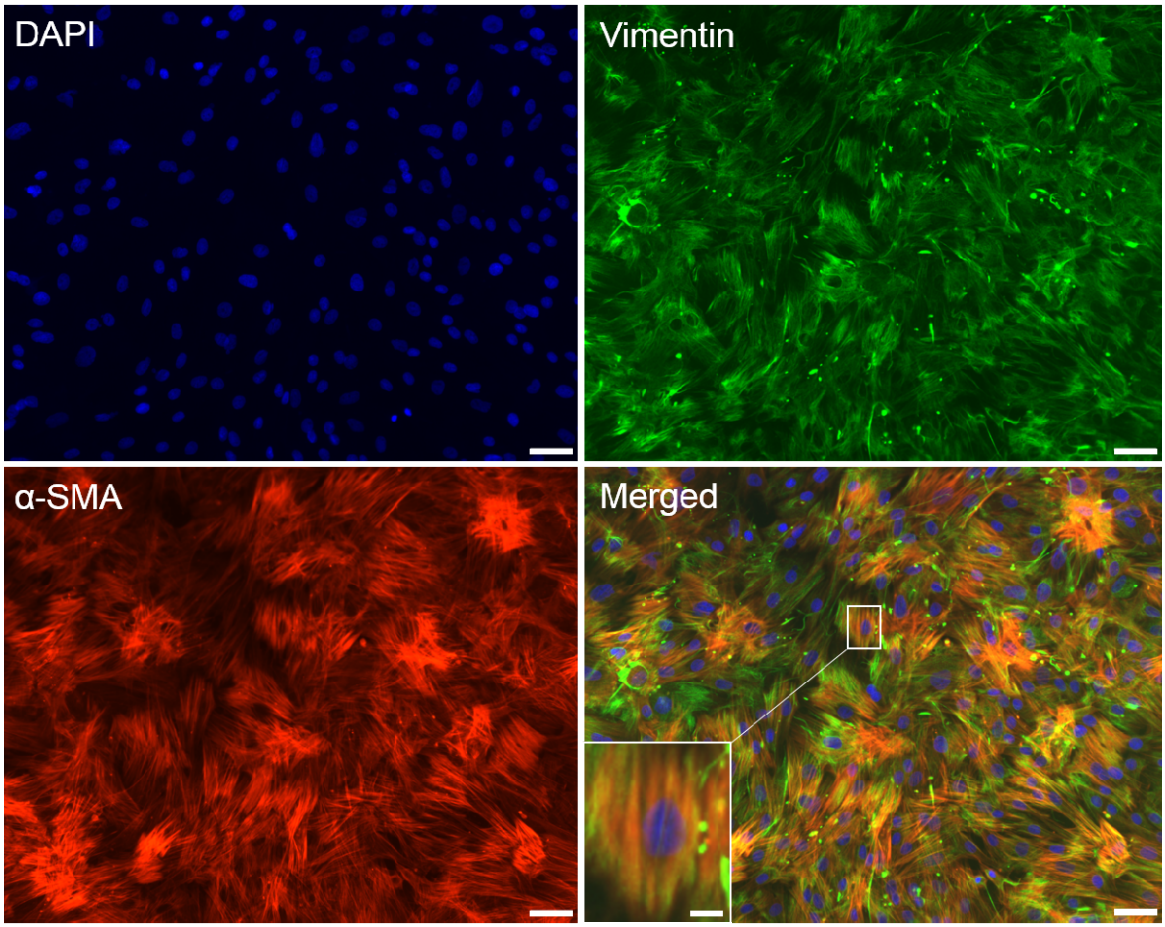

Representative fluorescent photomicrographs taken from culture shows colocalization of α-smooth muscle actin and vimentin in individual cells. Nuclei were counterstained with DAPI as above. Double-labeled cells appear in orange on merged picture indicating that most of smooth muscle cells differentiated into myofibroblasts. 20x magnification. Scale bars = 50 µm. Inlet scale bar = 10 µm.

Supplemental Figure III - Confocal microscopy.

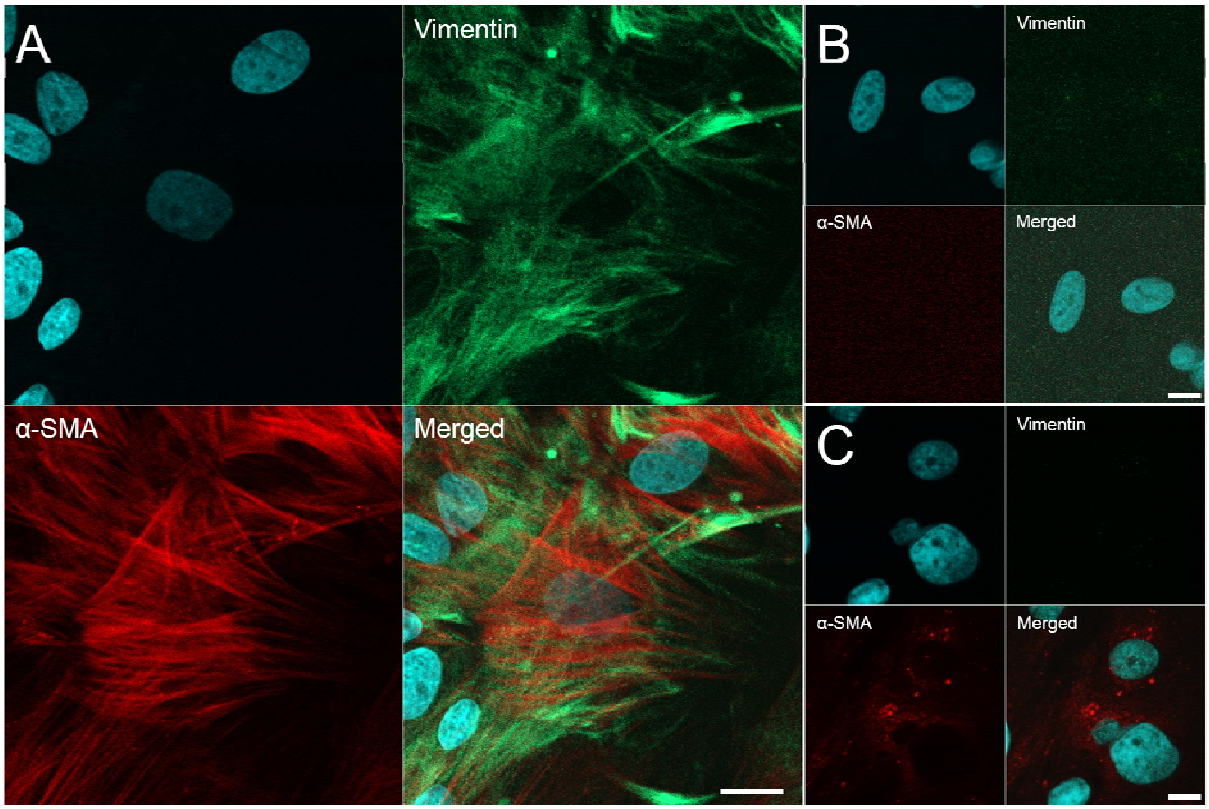

Fluorescence confocal photomicrographs of smooth muscle cells after twelve passages in culture. Nuclei were counterstained with DAPI (blue). The synthetic phenotype of smooth muscle cells (A) was confirmed by immunostaining for α-smooth muscle actin (red) and vimentin (green) filaments. Negative controls were performed in unlabelled (B) and CM-DiI-labeled (C) cell cultures. 40x magnification. Scale bars = 10 μm.

Supplemental Figure IV - MRA recanalization grading system.

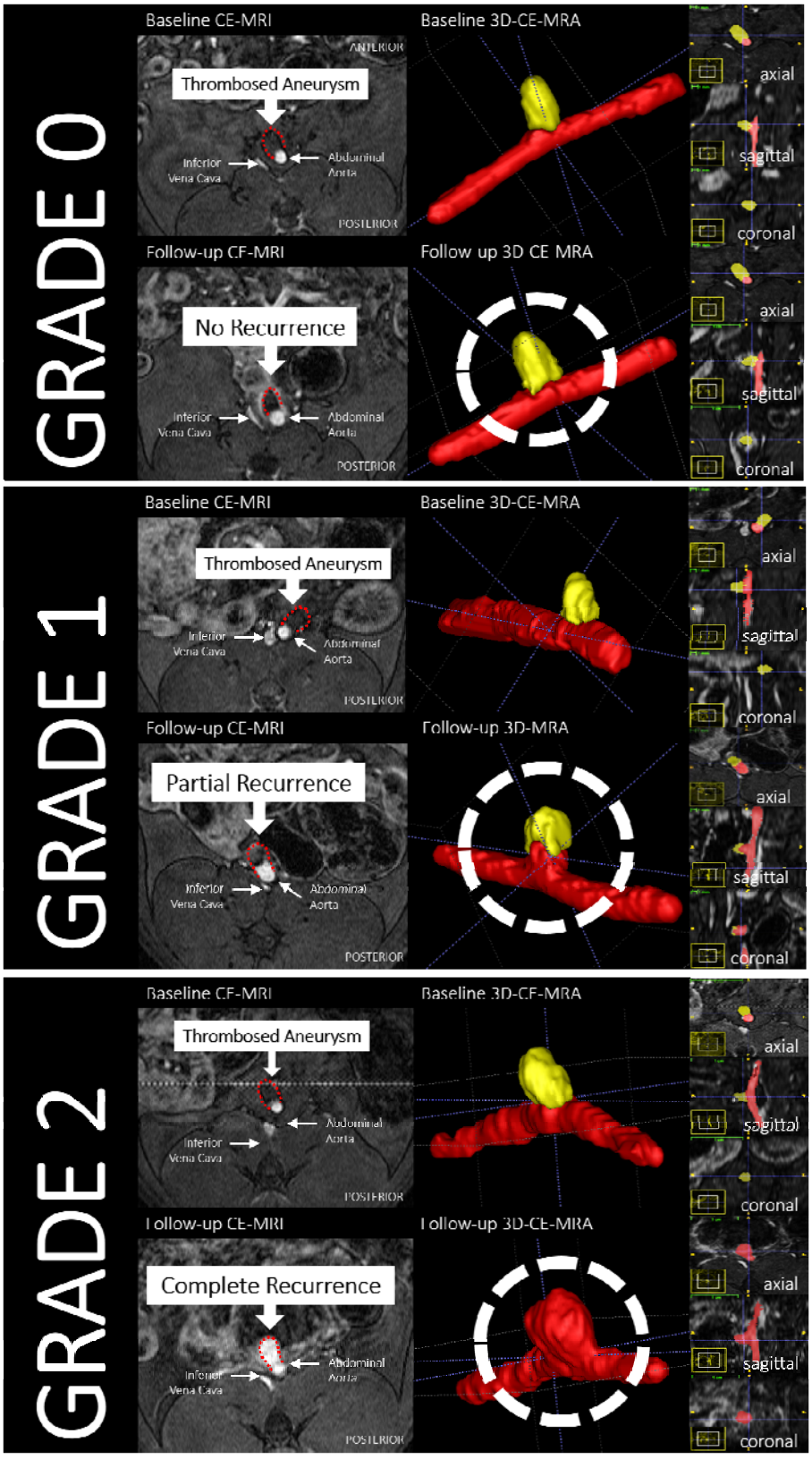

The dotted red line on axial CE-MRI represents the boundary of the aneurysm within the abdominal cavity. Aneurysm recurrence was categorized on contrast filling as highlighted by the white bold-dashed circle: 0 = no recurrence (no filling); 1 = partial recurrence (< 50% filling); 2 = complete recurrence (> 50% filling). Vessel and aneurysm lumen filling with contrast is color-coded in red, thrombosed areas in yellow.

Supplemental Figure V - Neointima score.

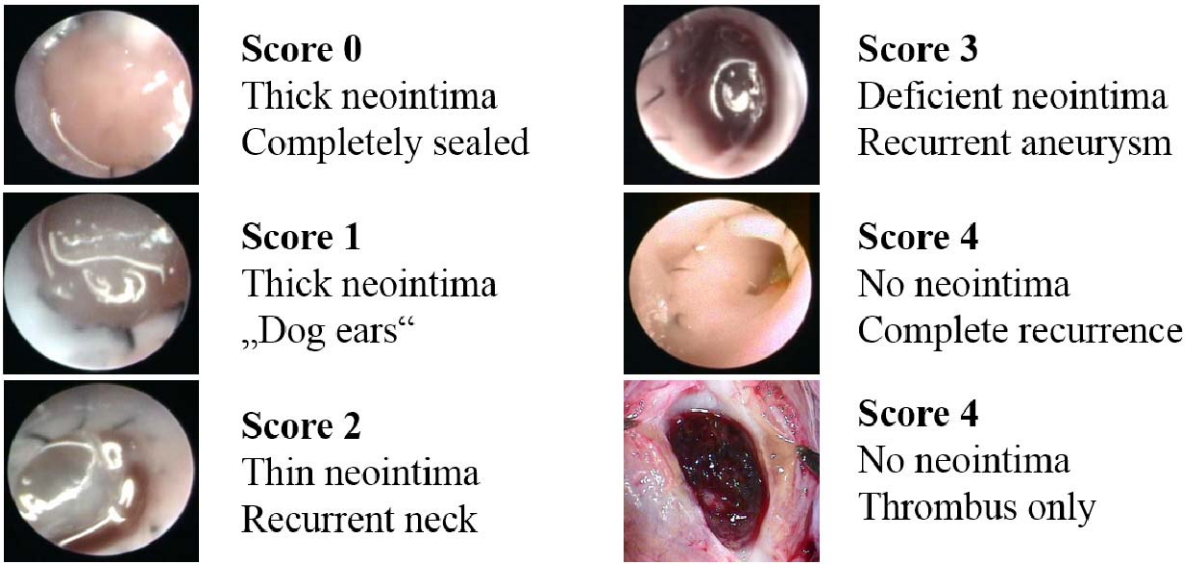

Score 0 = thick neointima, no recanalization, completely sealed; Score 1 = thick neointima, minimal recanalization “dog ears”; Score 2 = thin neointima covering completely, crescentic recanalization; Score 3 = deficient neointima or neointima only partially covering the aneurysm orifice, recurrent aneurysm; Score 4 = no neointima but only thrombus or complete recanalization. With the exception of three videos in the TD group (see Supplemental Figure VII), all recordings provided high-quality images at day three after aneurysm creation.

Supplemental Figure VI - Screenshots OPT videos

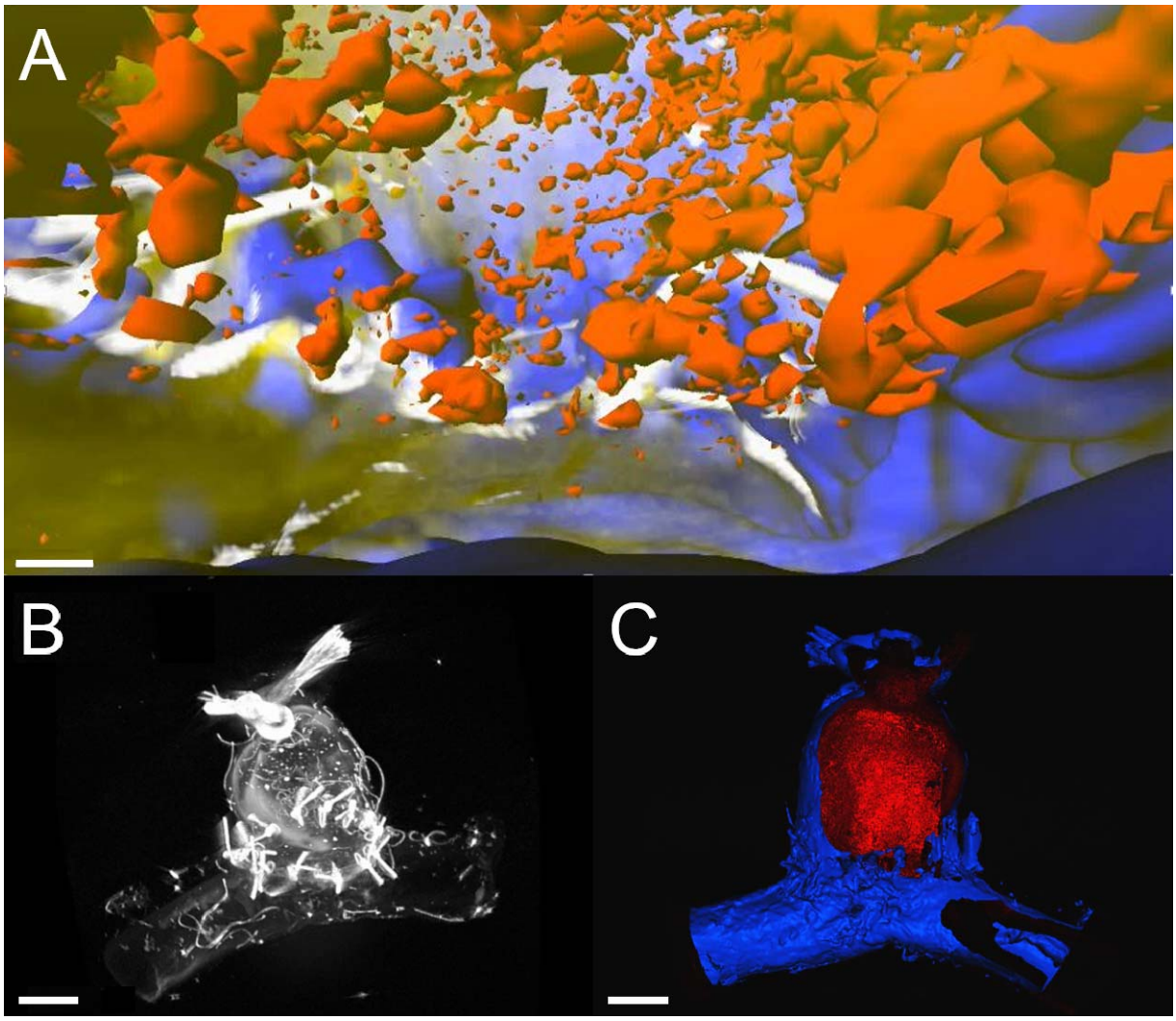

(A) Screenshot from high resolution 3D fly-through animation peering inside a cell transplanted aneurysm, view from parent artery bottom to top. The suture material at the aneurysm orifice appears white (white light filter), the aneurysm and vessel wall is depicted in blue (FITC-lectin staining; GFP+ filter), the fibrin biopolymer induced thrombus is visualized translucent yellow (auto fluorescence; GFP1 filter), and the transplanted cells appear as red objects (CM-Dil; TXR filter). Scale bar = 200 µm. (B) General 3D anatomical morphology of a sidewall aneurysm. Scale bar = 1mm. (C) The clipping plane through the isosurface rendered vessel wall (FITC-lectin staining; GFP+ filter, blue) reveals internal morphology of the aneurysm and parent artery. The section demonstrates intra-aneurysmal biopolymer embedded cell grafts (CM-Dil; TXR filter, red). Scale bar = 1mm. (Supplemental Movie II)

Supplemental Figure VII - Case by case CE-MRA, endoscopic and macroscopic findings.

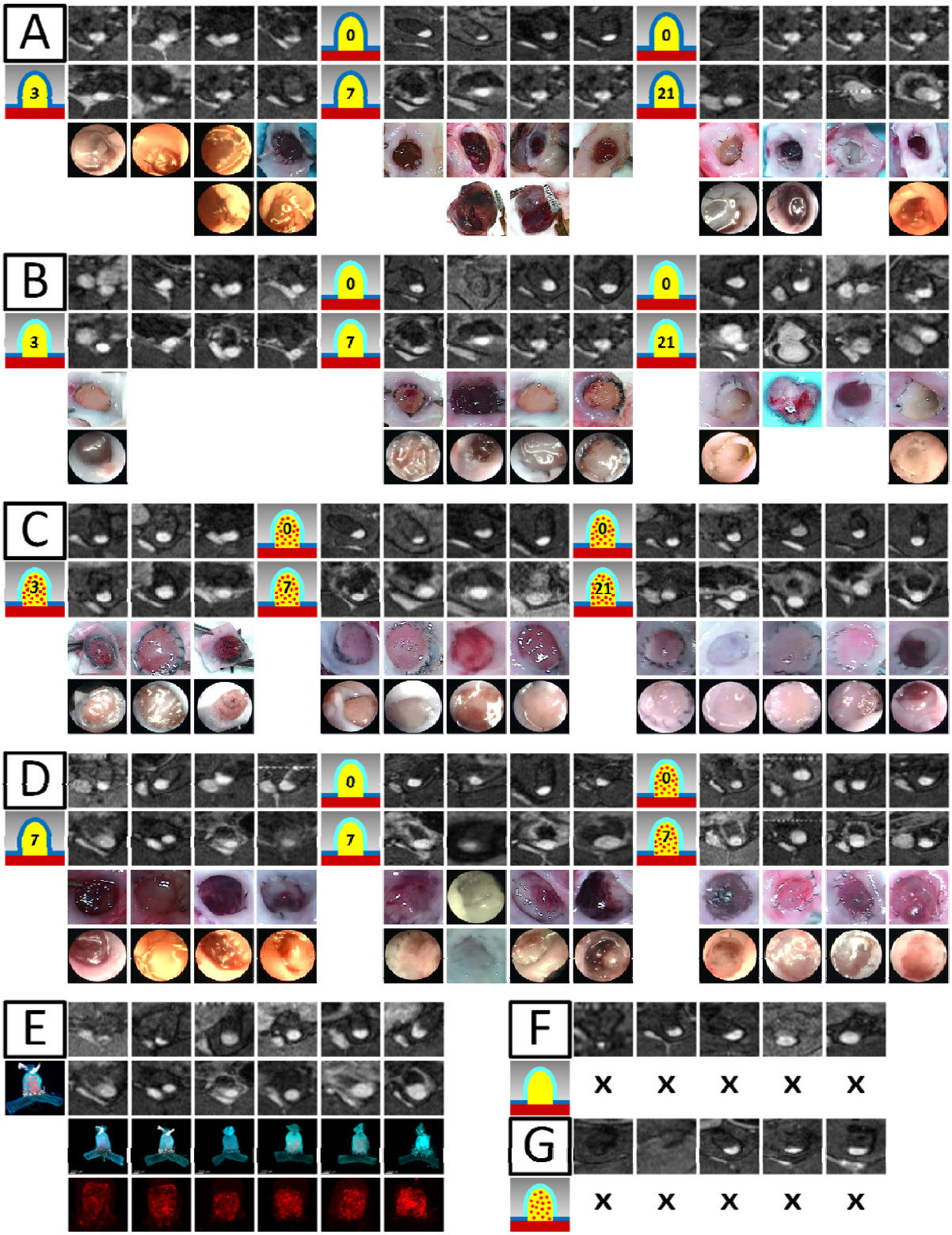

(A) TN - Thrombus-induced non-decellularized aneurysms. (B) TD - Thrombus-induced decellularized aneurysms. (C) TDTx - Thrombus-induced decellularized cell transplanted aneurysms. (D) Replicate on day 7 TN, TD, and TDTx. (E) Optical projection tomography of TDTx on day 0, 3, and 7. (F) Baseline CE-MRA of TD drop outs. (G) Baseline CE-MRA of TDTx drop outs.

Supplemental Figure VIII - Aneurysm growth.

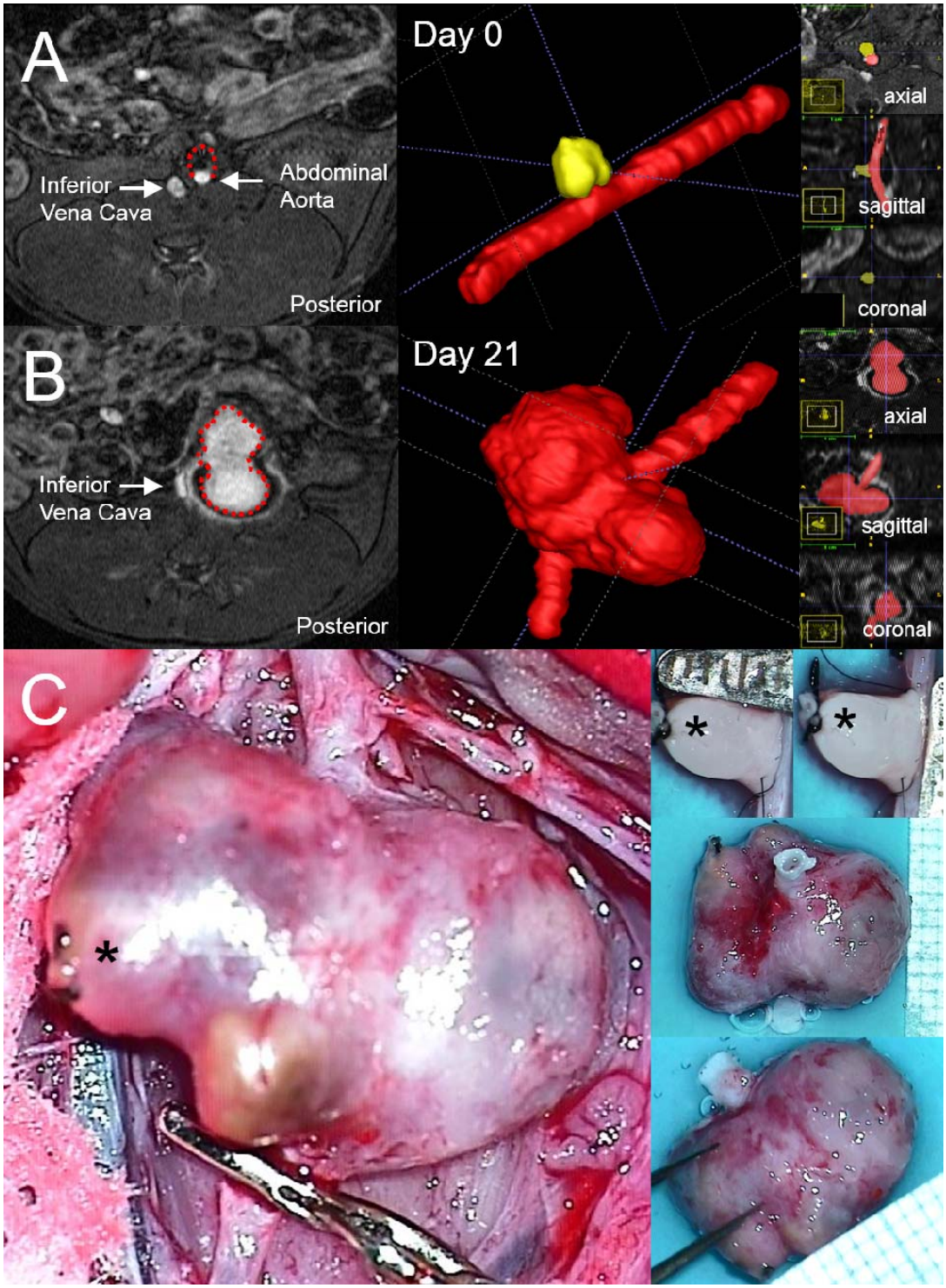

(A) Baseline CE-MRA and reconstructed 3D-CE-MRA on day O after surgery demonstrates complete aneurysm embolization. (B) Follow-up imaging on day 21 reveals significant growth into a giant multilobulated aneurysm. (C) Intraoperative screenshot during aneurysm harvesting (the distal abdominal aorta is clamped). The upper two panels on the right demonstrate aneurysm dimensions at baseline (3.0 x 2.5 mm, scale of ruler = 0.5 mm). The middle and lower right panels demonstrate dimensions at follow-up (14 x 13 mm, scale of ruler = 1 mm). * - indicates ligature at the dome of the aneurysm. (Supplemental Movie I)

Supplemental Figure IX - Characteristics of growing aneurysm.

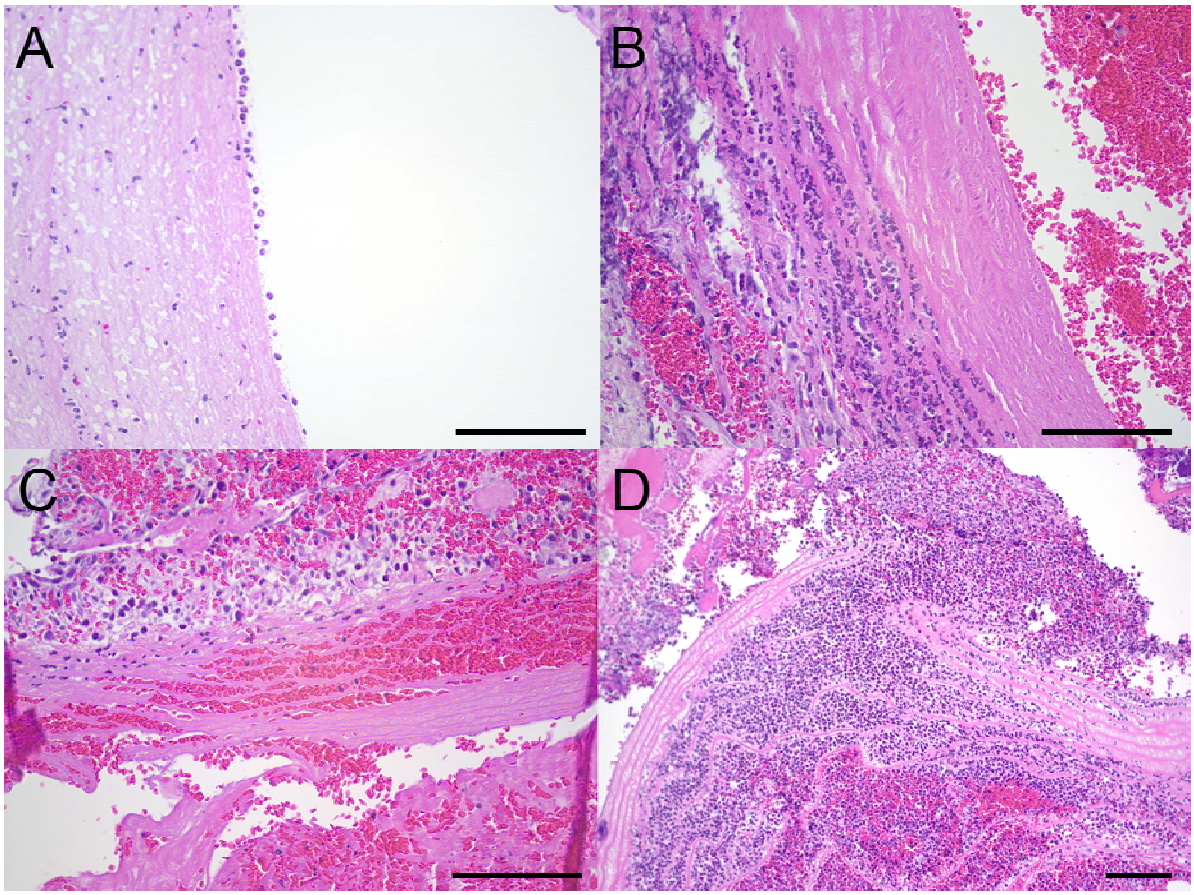

(A) Endoluminal neutrophil accumulation attached to the surface of the thrombus “neutrophil fishing”; 20x magnification; scale bar = 100 µm. (B) Neutrophils infiltrating the decellularized wall; 20x magnification; scale bar = 100 µm. (C) Mural hematoma; 20x magnification; scale bar = 100 µm. (D) Complete wall disruption; 10x magnification; scale bar = 50 µm.

Supplemental Figure X - Histological findings of all experimental groups.

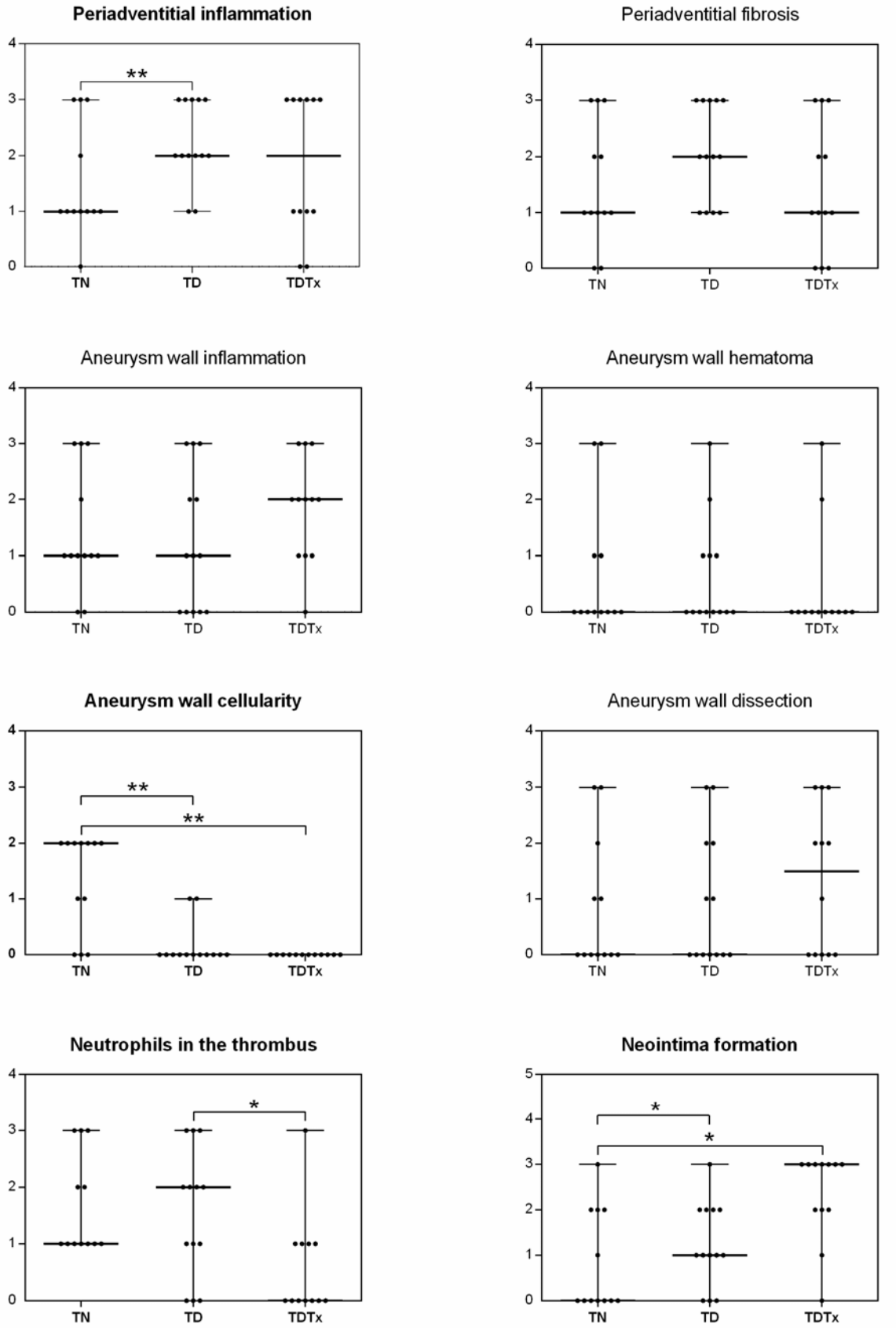

TN – Thrombus-induced non-decellularized aneurysms (n = 12). TD – Thrombus-induced decellularized aneurysms (n = 13). TDTx – Thrombus-induced decellularized and cell transplanted aneurysms (n = 12). * $P < 0.05$; ** $P < 0.01$.

Supplemental Table I - Surgical characteristics.

Experimental groups	TN-3 (n = 4)	TN-7 (n = 4)	TN-21 (n = 4)	TD-3 (n = 4)	TD-7 (n = 4)	TD-21 (n = 5)	TDTx-3 (n = 5)	TDTx -7 (n = 6)	TDTx -21 (n = 5)	RTN-7 (n = 4)	RTD-7 (n = 4)	RTDTx -7 (n = 4)
Mean body weight (grams)	387 ± 8	372 ± 3	362 ± 17	375 ± 50	434 ± 15	366 ± 15	294 ± 25	288 ± 14	354 ± 36	367 ± 16	305 ± 8	377 ± 18
Mean operation time (minutes)	61 ± 3	67 ± 23	71 ± 9	46 ± 6	54 ± 7	48 ± 8	50 ± 5	53 ± 5	52 ± 4	46 ± 5	48 ± 11	46 ± 10
Mean aortic clamping time (minutes)	25 ± 9	25 ± 6	23 ± 6	27 ± 5	24 ± 6	26 ± 6	30 ± 5	33 ± 3	32 ± 2	22 ± 6	26 ± 10	23 ± 8
Mean anastomosis time (minutes)	18 ± 5	22 ± 5	29 ± 15	19 ± 7	19 ± 5	16 ± 4	21 ± 4	24 ± 4	21 ± 4	15 ± 4	16 ± 5	24 ± 8
Mean time of hemostasis (minutes)	2 ± 2	2 ± 1	3 ± 3	1 ± 1	2 ± 1	2 ± 1	3 ± 4	3 ± 1	2 ± 1	3 ± 3	2 ± 2	3 ± 3
Median number of additional sutures	0 (0-1)	0 (0–1)	0	0 (0-3)	0 (0-1)	0 (0-1)	0 (0-2)	0	0	0 (0-1)	0	1 (0-1)
Mean graft ischemia time (minutes)	30 ± 11	29 ± 6	24 ± 5	NA	NA	NA	NA	NA	NA	25 ± 7	NA	NA
Mean aneurysm width (millimeter)	2.5 ± 0	2.5	24 ± 5	2.5	2.5	2.4 ± 0.1	2.5	2.5	2.5	2.4 ± 0.1	2.5	2.5
Mean aneurysm length (millimeter)	4 ± 0.4	3.9 ± 0.3	3.8 ± 0.3	3.9 ± 0.5	3.9 ± 0.8	3.5 ± 0.4	3.6 ± 0.5	3.4 ± 1.8	3.1 ± 0.3	3.6 ± 0.6	3.8 ± 0.3	3.4 ± 0.3

TN – Thrombus-induced non-decellularized aneurysms. TD – Thrombus-induced decellularized aneurysms. TDTx – Thrombus-induced decellularized and cell transplanted aneurysms. Prefix R – Replicate. NA – not applicable.

Supplemental Table II - Inflammatory findings of "healthy" aneurysms with mural cell loss.

Characteristic	Group	Scores				Dichotomized scores	
		0	1	2	3	0/1	2/3
Aneurysm wall inflammation*	L	0	1	1	3	1	4
	N	2	5	0	0	7	0
Neutrophils in thrombus**	L	0	1	0	3	1	4
	N	10	1	0	0	6	1

L – Healthy aneurysms with loss (no or only few) mural cells (n = 5).
N – Healthy aneurysms with focal hypocellularity or normal amount of mural cells (n = 7).
* $P = 0.01$ (Fisher`s exact test, two-tailed).
** $P = 0.072$ (Fisher`s exact test, two-tailed) ($P = 0.045$; one-tailed).

Supplemental Table III - Intrathrombus neutrophil accumulation in aneurysms with neointima formation.

Group	Neointima formation	Score neutrophils in thrombus				Dichotomized score neutrophils in thrombus	
		0	1	2	3	0/1	2/3
TN	O	0	3	0	1	3	1
	N	0	4	2	2	4	4
TD	O	2	2	1	0	4	1
	N	1	1	4	2	2	6
TDTx	O	9	0	0	1	10	0
	N	1	1	0	0	2	0
Overall*	O	11	5	1	2	16	3
	N	2	6	6	4	8	10

TN – Thrombus-induced non-decellularized aneurysms (n = 12). TD – Thrombus-induced decellularized aneurysms (n = 13). TDTx – Thrombus-induced decellularized and cell transplanted aneurysms (n = 12). O – Aneurysms with organizing neointima or mature neointima (n = 19; four TN, five TD, and ten TDTx). N – Aneurysms with no neointima or organizing thrombus (n = 18; eight TN, eight TD, and two TDTx). * $P = 0.017$ Overall O vs Overall N (Fisher`s exact test, two-tailed).

Supplemental Movies

Supplemental Movie I - Pulsating giant aneurysm at the time of harvest.

Supplemental Movie II - 3D fly-through animation of a cell transplanted aneurysm.

References

1. Marbacher S, Marjamaa J, Abdelhameed E, Hernesniemi J, Niemela M, Frosen J. The rat sidewall aneurysm model – the helsinki microsurgical aneurysm model. *Journal of visualized experiments : JoVE*. 2014;In press.

2. Marjamaa J, Antell H, Abo-Ramadan U, Hernesniemi JA, Niemela MR, Kangasniemi M. High-resolution tof mr angiography at 4.7 tesla for volumetric and morphologic evaluation of coiled aneurysm neck remnants in a rat model. *Acta Radiol*. 2011;52:340-348

3. Marbacher S, Marjamaa J, Bradacova K, von Gunten M, Honkanen P, Abo-Ramadan U, et al. Loss of mural cells leads to wall degeneration, aneurysm growth, and eventual rupture in a rat aneurysm model. *Stroke*. 2014;45:248-254